International Journal of Heat and Mass Transfer 52 (2009) 5954–5961

Contents lists available at ScienceDirect

International Journal of Heat and Mass Transfer

journal homepage: www.elsevier.com/locate/ijhmt

Natural convection cooling of a hot vertical wall wet by a falling liquid film

Gaetano Aiello, Michele Ciofalo *

Dipartimento di Ingegneria Nucleare, Università degli Studi di Palermo, Viale delle Scienze ed. 6, 90128 Palermo, Italy

ARTICLE INFO

Article history:
Received 27 June 2008
Accepted 6 August 2009
Available online 9 September 2009

Keywords:
Free convection
Liquid film
Humid air
Evaporative cooling
Containment cooling
Heat and mass transfer

ABSTRACT

The system studied is a plane channel in which one of the two vertical walls is kept at an arbitrary temperature profile and may be partially or completely wet by a falling liquid film, while the opposite wall is adiabatic. Air from the environment flows along the channel with a mass flow rate which depends on the balance between hydraulic resistances and buoyancy forces. These latter, in their turn, depend on the distribution of temperature and humidity (hence, density) along the channel and eventually on the heat and mass transferred from wall and film to the humid air.

A simplified computational model of the above system was developed and applied to the prediction of relevant quantities, such as the total energy subtracted to the hot wall, as functions of the geometrical and physical quantities that characterize the problem (channel height and thickness, localized hydraulic resistance, hot wall temperature and its distribution, film flow rate, ambient air temperature and humidity). Conclusions were also drawn on the cooling strategy to be adopted in the case when only a limited amount of coolant is available.

1. Problem description and modelling assumptions

1.1. Geometry and boundary conditions

The cooling of a hot vertical wall by a falling liquid film is a fundamental heat transfer problem, notably encountered in nuclear reactor safety. The case of high wall temperatures, dominated by sputtering and rewetting phenomena, has been studied for a long time in connection with the cooling of fuel rods and other core components [1]. In the present work we are interested in lower-temperature, larger-scale applications, typical, for example, of the Passive Containment Cooling System (PCCS) in AP600/AP1000 facilities [2]. Here, natural convection of air plays a crucial role and boiling, if any, occurs in the nucleate form well below DNB.

A full analysis of this problem requires an adequate modelling of the convection, condensation and evaporation phenomena occurring on either side of the containment, as well as of the thermal coupling between the inner and outer flow domains through the solid containment wall. System codes have usually been employed for this level of analysis [3]. Other studies have concentrated on the convection/evaporation phenomena occurring on the outer side. For example, Kang and Park [4] obtained experimental results for a wall wet by a falling liquid film; Yan [5] conducted a numerical study of the evaporative cooling of a falling liquid film in turbulent mixed-convection gas counter flow; and Arshavski et al. [6] included the effect of transient conjugate heat transfer involving conduction in the solid wall.

The purpose of the present work is to develop the simplest possible model of the outer-side evaporative cooling which still preserves the essential physics of the problem, thus allowing easy but meaningful parametrical studies. The computational domain is schematically shown in Fig. 1 and consists of a channel of height H and width s, delimited by two vertical walls. One of the walls is kept at an arbitrary temperature profile $T_w(x)$ and may or not be wet by a liquid film, which falls along it with an inlet temperature $T_{l,H}$ and an inlet mass flow rate $\Gamma_{l,H}$ p.u.l. (per unit length in the direction orthogonal to the plane of the figure). The opposite wall is adiabatic. Air from the environment, with inlet temperature T_0 and humidity m_0, flows along the channel with a mass flow rate p.u.l. Γ_a, driven by buoyancy forces.

This geometry can be thought of as approximating a cylindrical shell of negligible curvature, as in the AP600 containment cooling configuration. The inlet air mass flow rate $\Gamma_{a,0}$ depends on the distribution of air temperature T_a and humidity m (hence, density ρ_a) along the channel, which, in turn, depends on the heat and mass transfer between the hot wall (either dry or wet by a liquid film) and the humid air.

Besides the distributed frictional resistance of the channel, the air flow encounters a localized hydraulic resistance K, which may account also for the frictional losses in the air path upstream of the channel inlet and for the extra losses associated with entrance effects. The liquid film, if present, experiences a progressive reduction of its flow rate and thickness as it descends along the hot wall,

* Corresponding author.
E-mail address: ciofalo@din.unipa.it (M. Ciofalo).

0017-9310/$ - see front matter © 2009 Elsevier Ltd. All rights reserved.
doi:10.1016/j.ijheatmasstransfer.2009.08.007

Nomenclature

a, b	constants in the entrance effects multiplier for heat transfer, Eq. (19)
c_p	specific heat at constant pressure (J kg^{-1} K^{-1})
D_{eq}	hydraulic diameter, $2s$ (m)
E_T	thermal energy per unit perimeter (J m^{-1})
f	Darcy–Weisbach friction factor
Fr_τ	Froude number, $\tau_l/(\delta g \rho_l)$
g	acceleration due to gravity (m s^{-2})
h	convective heat transfer coefficient (W m^{-2} K^{-1})
h_m	convective mass transfer coefficient (kg m^{-2} s^{-1})
H	wall height (m)
J	specific enthalpy (J kg^{-1})
k_α	Kutateladze number of phase α, see Eq. (6)
K	localized hydraulic resistance coefficient
m	air humidity expressed as mass fraction
m''	water (humidity) mass flux from liquid film (kg m^{-2} s^{-1})
M	molar weight (kg mol^{-1})
p	pressure (Pa)
q''	heat flux (W m^{-2})
Q	mass per unit perimeter (kg m^{-1})
R	gas constant (J mol^{-1} K^{-1})
Re	Reynolds number
s	channel width (m)
t	time (s)
T	temperature (K)
u	velocity along x (m s^{-1})
W	power per unit perimeter (W m^{-1})
x	co-ordinate parallel to wall (m)
y	co-ordinate normal to the wall (m)

Greek symbols

Γ	mass flow rate per unit perimeter (kg m^{-1} s^{-1})
δ	liquid film thickness (m)
Δp	pressure variation (Pa)
θ	contact angle (°)
λ	thermal conductivity (W m^{-1} K^{-1})
μ	viscosity (Pa s)
ν	kinematic viscosity (m^2 s^{-1})
ρ	density (kg m^{-3})
σ	surface tension (N m^{-1})
τ	shear stress (Pa)
Ψ	molar (and partial pressure) ratio

Subscripts and superscripts

a	humid air
boil	boiling
buo	buoyancy
conv	convective
crit	critical value for flooding
DNB	departure from nucleate boiling (critical heat flux)
eff	effective
evap	evaporative
f, g	saturated liquid and saturated vapour
H	channel top
l	liquid film
loss	frictional loss
max	maximum
ref	reference
sat	saturation
v	(water) vapour
w	wall
wet	wetting
δ	liquid film edge
0	channel bottom = environment
*	liquid film dry-out location

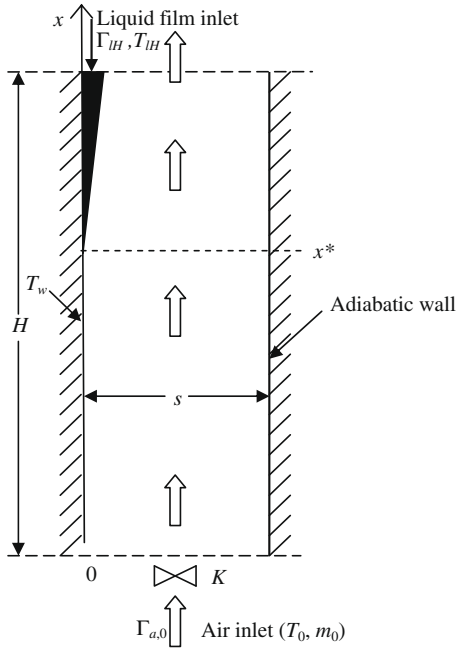

Fig. 1. Schematic of the physical system.

due to evaporative or boiling mass transfer to the humid air flow, and may be completely dried out at a height x^*.

1.2. Characteristics and stability of the liquid film

Consider the directions of motion indicated in Fig. 2(a). By assuming laminar flow conditions for the liquid film, writing its equations of motion (which reduce themselves to a balance between gravity and viscous forces) and imposing the no slip condition at the wall ($y = 0$) and a shear stress τ_l at the film–air interface ($y = \delta$), the following dimensionless velocity profile inside the film is obtained:

$$\frac{u_l(y)}{u_{l,0}} = \frac{y}{\delta}\left(1 - \frac{1}{2}\frac{y}{\delta}\right) - Fr_\tau \frac{y}{\delta} \tag{1}$$

in which g is the gravity acceleration, ρ_l and ν_l are the liquid density and kinematic viscosity, δ is the film thickness, $u_{l,0} = (g\delta^2)/\nu_l$ and Fr_τ is the film Froude number based on the interfacial shear stress τ_l and on the film thickness δ, $Fr_\tau = \tau_l/(g\delta\rho_l)$.

Fig. 2(b) shows dimensionless profiles given by Eq. (1) for different values of the Froude number. Note that the case $Fr_\tau = 0$ corresponds to the no shear condition $\tau_l = 0$.

By integrating Eq. (1), the following expression is obtained for the mass flow rate Γ_l of the liquid film as a function of thickness and Froude number:

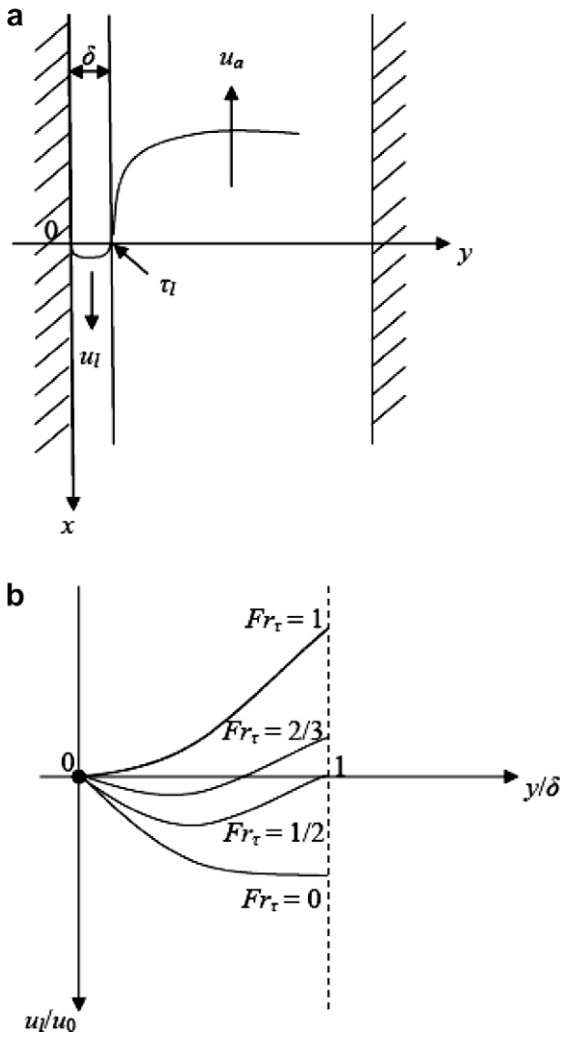

Fig. 2. Liquid film behaviour. (a) Shear stress at the film–air interface. (b) Dimensionless velocity profiles across the film for different values of the Froude number ($Fr_\tau = 0$: no shear; $Fr_\tau = 2/3$: no net flow rate).

$$\Gamma_l = \frac{\rho_l}{\nu_l}\delta^3 g\left(\frac{1}{3} - \frac{1}{2}Fr_\tau\right) \tag{2}$$

Note that the case $Fr_\tau = 2/3$ corresponds to $\Gamma_l = 0$.

Now, for equilibrium reasons τ_l must be equal to the shear stress τ_a that acts on the film surface from the air side. This can be roughly estimated as a function of the mean air speed and channel thickness s by using turbulent flow correlations, e.g., Blasius. For example, for ambient air, a mean air speed of 1 m s^{-1} and $s = 0.2$ m, one has $\tau_a \approx 3.8 \times 10^{-3}$ N m^{-2}. The Froude number is then $Fr_\tau \approx 3.9 \times 10^{-7}/\delta$, showing that $Fr_\tau \ll 1$ for realistic values of the film thickness δ. Therefore, the prevailing conditions are close to *no-shear* ones ($Fr_\tau = 0$) and Eq. (2) yields a film thickness:

$$\delta \approx \left(\frac{3\Gamma_l \nu_l}{\rho_l g}\right)^{1/3} \tag{3}$$

For example, for $\Gamma_l = 0.2$ kg m^{-1} s^{-1}, one has $\delta \approx 4 \times 10^{-4}$ m at ambient temperature. For the liquid film velocity, Eq. (1) yields in the no-shear case:

$$u_{l,\max} = \frac{g\delta^2}{2\nu_l} \tag{4}$$

($\sim$0.8 m/s for $\Gamma_l = 0.2$ kg m^{-1} s^{-1} at ambient temperature). From Eqs. (3) and (4), the film Reynolds number based on film thickness and maximum liquid speed, $Re_{max} = u_{l,max}\delta/\nu_l$, can be expressed as:

$$Re_{max} = \frac{3}{2}\frac{\Gamma_l}{\mu_l} \tag{5}$$

($\sim$300 for $\Gamma_l = 0.2$ kg m^{-1} s^{-1}). Therefore, the assumption of laminar flow is justified and Eq. (3) can be used to evaluate the film thickness δ.

However, the possibility of film *flow reversal* or *flooding* under the action of the counter-flow air, as well as the possibility of the film breaking up into *rivulets*, must be considered.

(a) As regards *flow reversal*, for any geometry and liquid–gas couple the condition $\Gamma_l = 0$ (Fig. 2b) corresponds to $Fr_\tau = 2/3$ and, as discussed above, can safely be ruled out for realistic values of the air speed.

(b) *Flooding* may occur due to the propagation and amplification of oscillatory instabilities at the film–air interface. Commonly used correlations for the occurrence of flooding conditions [7] are based on the Kutateladze number of both phases:

$$k_\alpha = \bar{u}_\alpha\left[\frac{\rho_\alpha^2}{g\sigma(\rho_l - \rho_\alpha)}\right]^{1/4} \tag{6}$$

in which α denotes liquid (l) or gas (a) phase, the overbar denotes averaging over the liquid or gas cross section, and σ is the surface tension. The flooding condition can be expressed as:

$$k_a^{1/2} + Ak_l^{1/2} = B \tag{7}$$

For example, Pushkina and Sorokin [8] suggest $A = 0$ and $B = 1.79$, which yields a simple flooding criterion involving only the gas-phase speed:

$$k_{a,crit} = 3.2 \tag{8}$$

For the present air–water system, if the physical properties are evaluated at the ambient temperature of 20 °C ($\sigma = 72.8 \times 10^{-3}$ N m^{-1}, $\rho_l \approx 10^3$ kg m^{-3}, $\rho_a \approx 1.25$ kg m^{-3}) one has $ka \approx 0.216\bar{u}_a$ and Eq. (8) predicts flooding only if the mean air speed exceeds the value of $\sim$15 m s^{-1}. Preliminary calculations show that, for the problem under consideration, the expected air speeds are much lower than the above value, so that the possibility of flooding by hydrodynamic instability can be safely ruled out.

The breaking of a liquid film into *rivulets* may be triggered by surface wave instability or thermocapillary instability [9]. The latter mechanism occurs only on heated surfaces, while the former may occur also in isothermal flows. As regards surface-wave instability, film breakup may be thought to occur when the theoretical film thickness decreases below a minimum thickness δ_{min} which depends on the fluid's and the surface's properties and on the wall inclination angle; for example, for vertical walls El-Genk and Saber [10] propose the approximate criterion

$$\Delta_{min} = (1 - \cos\theta)^{0.22} \tag{9}$$

in which θ is the contact angle and Δ is the dimensionless film thickness, defined as

$$\Delta = \delta\left(\frac{\rho_l^3 g^2}{15\mu_l^2\sigma}\right)^{1/5} \tag{10}$$

For water–steel contact, which would be typical of the AP600 containment, the contact angle θ ranges between 70° and 90° [11]. Using (conservatively) this upper value, the physical properties of water and Eqs. (9) and (10), the minimum film thickness δ_{min} is found to be $\sim$0.4 mm at 20 °C and $\sim$0.25 mm at 100 °C. These values are of the same order as those obtained for δ from Eq. (3) for realistic value of the water flow rate; therefore, the possibility of film breakdown and rivulet formation cannot be ruled out under the present conditions. This is even more true if the simultaneous occurrence of the second type of instability (*thermocapillary*), for which no simple correlation was found in the literature, is taken into account.

For the sake of simplicity, in the present study we ignore the possible presence of rivulets and assume that the liquid film, if present, covers the wall uniformly from $x = H$ to the dry-out height $x = x^*$. As a *caveat*, it should be observed that this is not a conservative assumption, since the presence of dry patches would reduce the overall wall cooling rate.

1.3. Summary of the modelling assumptions

Taking the above considerations into account, the overall modelling assumptions can be summarized as follows:

- Steady state conditions hold.
- The wall temperature T_w is a known boundary condition, possibly function of the axial location x. Of course, this assumption makes heat conduction in the wall thickness irrelevant. Should heat transfer through the wall be explicitly modelled, it can be anticipated that *longitudinal* heat conduction would play a minor role in reactor-scale applications due to the large value of the longitudinal Biot number $(H^2h)/(s_w\lambda_w)$ [12], in which H, s_w and λ_w are the height, thickness and thermal conductivity of the wall and h is the overall heat transfer coefficient. Therefore, the outer wall temperature would depend mainly on the *local* balance between the heat transferred to the inner surface of the wall (e.g., by condensation) and that removed from the outer surface by convection, evaporation or boiling.
- The thermal resistance of the liquid film is equal to its conductive value δ/λ_l (see Section 2.2).
- Film flow reversal and flooding do not occur, which puts limits to the air velocity (see Section 1.2).
- The liquid film covers the wall uniformly, i.e., no *rivulets* form (see, however, Section 1.2).
- The system pressure is uniform and equal to the ambient pressure p_0.
- Boiling, if present ($T_w > T_{sat}$), is nucleate (which implies $T_w < T_{DNB}$).
- The air flow is turbulent and perfectly mixed (air temperature and humidity are functions of x only). The assumption of turbulent air flow is amply justified *a posteriori* (i.e., by the computed values of its flow rate) provided the gap thickness s, the wall height H and the difference between wall and ambient temperature $T_w - T_0$ are sufficiently large. For example, even for $s = 0.1$ m, $H = 20$ m and $T_w - T_0 = 40$ K (which are all very small values for a full-scale plant), the air Reynolds number is well above 20,000.
- Although the air flow is driven by buoyancy forces, forced-convection correlations can be approximately used both for friction and for heat/mass transfer due to the high aspect ratio of the channel ($H/s \gg 1$).

2. Governing equations

2.1. Balance equations

With reference to Fig. 1, the *conservation* equations which govern the phenomenon are:

- Humid air mass balance (constant dry air flow, variable water component flow):

$$\frac{\partial \Gamma_a}{\partial x} = \frac{\partial (m\Gamma_a)}{\partial x} = m'' \tag{11}$$

- Liquid film mass balance (if appropriate):

$$\frac{\partial \Gamma_l}{\partial x} = m'' \tag{12}$$

- Humid air enthalpy balance:

$$\frac{\partial J_a}{\partial x} = q'' \tag{13}$$

- Humid air flow momentum balance, including buoyancy, pressure losses and inlet–outlet momentum change:

$$\Delta p_{buo} - |\Delta p_{loss}| = \frac{\Gamma_{a,H}^2}{\rho_{a,H} s^2} - \frac{\Gamma_{a,0}^2}{\rho_{a,0} s^2} \tag{14}$$

in which the driving buoyancy term and the overall loss term are given by:

$$\Delta p_{buo} = \int_0^H (\rho_{a,0} - \rho_a) g \, dx \tag{15}$$

$$|\Delta p_{loss}| = \int_0^H f \frac{1}{2 D_{eq} \rho_a} \left(\frac{\Gamma_a}{s}\right)^2 dx + K \frac{1}{2\rho_{a,0}} \left(\frac{\Gamma_{a,0}}{s}\right)^2 \tag{16}$$

respectively, $D_{eq} = 2s$ being the hydraulic diameter of the channel. The friction coefficient is computed by the Blasius correlation ($f = 0.316 Re^{-0.25}$); entrance effects are not explicitly computed but rather included in the singular pressure loss constant K.

2.2. Kinetic equations

As regards heat and mass transfer correlations (*kinetic* equations), the total heat flux from hot wall to humid air flow is expressed in the most general case as:

$$q'' = q''_{conv} + q''_{evap} + q''_{boil} \tag{17}$$

- The convective heat flux q''_{conv} is always present and is computed as:

$$q''_{conv} = h(T_\delta - T_a) \tag{18}$$

in which T_δ is the temperature at the film–air interface and the convective coefficient h is computed by the Dittus–Bölter correlation modified for entrance effects:

$$\frac{h D_{eq}}{\lambda_a} = 0.023 \left(\frac{\Gamma_a D_{eq}}{\mu_a s}\right)^{0.8} \left(\frac{c_{p,a}\mu_a}{\lambda_a}\right)^{0.4} \left[1 + a \exp\left(-b \frac{x}{D_{eq}}\right)\right] \tag{19}$$

(see Section 3.1 for the values of the dimensionless constants a and b).

- Evaporative heat and mass transfer exist only in the presence of the liquid film. The evaporative mass flux is computed as:

$$m''_{evap} = h_m (m_\delta - m_{eff}) \tag{20}$$

in which $m_\delta = m_{sat}(T_\delta)$ is the humidity at the film surface and $m_{eff} = \min[m, m_{sat}(T_a)]$. For the mass transfer coefficient h_m the heat/mass transfer analogy is used [13]:

$$h_m \cong \frac{h}{c_{p,a}} \tag{21}$$

where, in the absence of reliable correlations, the specific heat of humid air is approximated by that of dry air. The evaporative film–air heat flux is then computed as:

$$q''_{evap} = m''_{evap} J_g \tag{22}$$

in which J_g is the enthalpy of saturated vapour at the wall (and liquid film) temperature.

In Eqs. (18) and (20) T_δ is a further unknown, but can be obtained by imposing the total heat flux $q''_{conv} + q''_{evap}$ to coincide with the heat flux crossing the film:

$$q''_{conv} + q''_{evap} = (T_w - T_\delta)\lambda_l/\delta \tag{23}$$

Eqs. (18)–(23) are solved numerically for q''_{conv}, q''_{evap} and T_δ by means of an iterative technique.

- Boiling heat and mass transfer are present only for $T_w > T_{sat}$ (and, of course, in the presence of the liquid film). The boiling mass flux is computed by the Jens and Lottes correlation [9]:

$$m''_{boil} \cong \frac{f(p)}{J_{fg}}(T_w - T_{sat})^4 \tag{24}$$

in which $f(p) = 2.73$ (SI units) at atmospheric pressure. The boiling film–air heat flux is then computed, by analogy with the evaporative one, as:

$$q''_{boil} = m''_{boil} J_g \tag{25}$$

When boiling is present, the film is assumed to be at the uniform temperature T_{sat} and Eqs. (18) and (20) are modified accordingly, while Eq. (23) is not used. Note that boiling heat fluxes as given by Eq. (25) are usually far larger than evaporative and convective ones.

2.3. Thermodynamic equations and physical properties

The humidity m, defined as the water/mixture mass ratio, is related to the molar (and partial pressure) ratio ψ by:

$$\frac{1}{\psi} = \left(1 - \frac{M_l}{M_a}\right) + \frac{1}{m}\frac{M_l}{M_a} \tag{26}$$

in which $M_l = 18.016 \times 10^{-3}$ kg mol^{-1} and $M_a = 28.978 \times 10^{-3}$ kg mol^{-1} are the molar weights of water and standard air, respectively [15]. The saturation humidity m_{sat} is attained when the partial pressure of water vapour equals the saturation pressure of water at the humid air temperature T_a, i.e., when $\psi = p_{sat}(T_a)/p_0$; Eq. (26) thus yields:

$$m_{sat}(T_a) = \frac{M_l}{M_a}\left[\frac{p_0}{p_{sat}(T_a)} - \left(1 - \frac{M_l}{M_a}\right)\right]^{-1} \tag{27}$$

The following approximate correlations were used in the calculations to compute the saturation temperature $T_{sat}(p)$, the saturation pressure $p_{sat}(T)$ and the latent heat of vaporization of water $J_{fg}(T)$:

$$T_{sat} = 0.1323(\ln p)^3 - 2.2303(\ln p)^2 + 26.8396(\ln p) + 157.53 \tag{28}$$

$$p_{sat} = 1.9657 \times 10^{-6}T^5 - 2.1785 \times 10^{-3}T^4 + 0.9168T^3 - 174.21T^2 + 1.2872 \times 10^4 T - 6.3497 \times 10^4 \tag{29}$$

$$J_{fg} = -2.49T^2 + 820.5T + 2.91 \times 10^6 \tag{30}$$

(p and p_{sat} in Pa, T and T_{sat} in K, J_{fg} in J kg^{-1}), valid for $p = 611$–4.76×10^5 Pa or $T = 273.15$–423.15 K, i.e., 0–150 °C). Eqs. (28)–(30) approximate the data from the UK Steam Tables [16] to within ~1% over most of the range of interest. The enthalpy of saturated vapour was then computed as:

$$J_g(T) = c_{p,l}[T - T_{ref}] + J_{fg}(T) \tag{31}$$

with $c_{p,l} = 4186$ J kg^{-1} K^{-1} and $T_{ref} = 273.15$ K (0 °C). The enthalpy of superheated vapor was computed as:

$$J_v(T, p_v) = J_g(T_{sat}(p_v)) + c_{p,v}[T - T_{sat}(p_v)] \tag{32}$$

with $c_{p,v} = 1870$ J kg^{-1} K^{-1} at atmospheric pressure [16]. The total enthalpy of humid air was computed by the formulae:

$$J_a = [1 - m]c_{p,a}[T_a - T_{ref}] + mJ_g(T_{sat}(p_v)) + mc_{p,v}[T_a - T_{sat}(p_v)] \tag{33}$$

$$J_a = [1 - m]c_{p,a}[T_a - T_{ref}] + m_{sat}J_g(T_a) + [m - m_{sat}]c_{p,l}[T_a - T_{ref}] \tag{34}$$

valid for undersaturated air ($m \leqslant m_{sat}$) and oversaturated air ($m > m_{sat}$), respectively. Similarly, the density of humid air was computed by the formulae:

$$\rho_a(m, T) = 10^{-3}\frac{p_0}{RT}\left[\frac{1 - m}{M_a} + \frac{m}{M_l}\right]^{-1} \tag{35}$$

$$\rho_a(m, T) = 10^{-3}\frac{p_0}{RT}\left[\left(\frac{1 - m}{M_a} + \frac{m_{sat}}{M_l}\right) + \frac{m - m_{sat}}{\rho_l}\right]^{-1} \tag{36}$$

valid for undersaturated air ($m \leqslant m_{sat}$) and oversaturated air ($m > m_{sat}$), respectively.

2.4. Energy balance

The energy balance of the system considered is schematically shown in Fig. 3 for the general case in which a residual liquid water film flow $\Gamma_{l,0}$ reaches the base of the wall. It should be observed that the power per unit perimeter W_a absorbed by the humid air flow:

$$W_a = \Gamma_{a,H}J_{a,H} - \Gamma_{a,0}J_{a,0} \tag{37}$$

differs, in general, from the power W_w subtracted to the hot wall and satisfies:

$$W_w = W_a - (\Gamma_{l,H}J_{l,H} - \Gamma_{l,0}J_{l,0}) \tag{38}$$

where $J_{l,H}$ and $J_{l,0}$ are the enthalpies of the liquid water film at the top and bottom of the wall.

2.5. Discretization and numerical solution

The above equations were discretized by the finite-volume method and numerically solved by a purpose written Fortran code.

In principle, it would be possible to choose a value of the inlet film flow rate $\Gamma_{l,H}$ and compute the dry-out location x^* as part of the solution. However, an iterative approach would then be necessary since the dry/wet status of the wall at a generic height would not be known *a priori*. It was found easier to loop on the film dry-out height x^* (from 0 to H) and compute for each value of x^* both the film and the air flow rates. A simple iterative procedure was still necessary to compute the air flow rate satisfying the balance between buoyancy forces, pressure losses and inlet–outlet momentum change, Eqs. (14)–(16), and a separate iterative loop was required at each axial location to solve Eqs. (18)–(23), as discussed in Section 2.2.

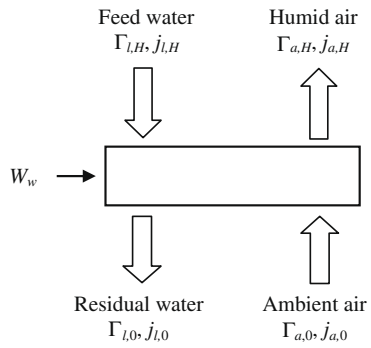

Fig. 3. Energy balance of the physical system.

3. Tuning and validation

3.1. Entrance effects and validation for the case of a dry wall

For the case of a dry wall ($x^* = H$), results were compared with 2D predictions obtained by using the CFX-4 CFD code [17], the $k-\varepsilon$ turbulence model and the Boussinesq approximation for buoyancy, and modelling also the air paths upstream and downstream of the computational domain in Fig. 1. A satisfactory agreement was obtained by setting $a = 1.5$, $b = 0.18$ in Eq. (19) and $K = 5$ in Eq. (16). For example, Fig. 4 compares profiles of the wall heat flux predicted for $H = 30$ m, $s = 0.2$ m, $T_0 = 20$ °C and three values of the wall temperature T_w (40, 60 and 100 °C).

3.2. Validation for the case of a completely wet wall

For the case of a completely wet wall ($x^* = 0$), results were compared with experimental data obtained by Kang and Park [4] in a 2 m high test section. Since the authors used forced convection to establish a given flow rate, the present computational procedure was slightly modified so that this quantity was imposed, rather than computed as part of the solution. The above values of the entrance effects constants ($a = 1.5$, $b = 0.18$) were used. For example, Fig. 5 compares average wall heat transfer coefficients predicted for $H = 2$ m, $s = 0.1$ m, $T_0 = 25$ °C and three values of the wall temperature T_w (50, 60 and 70 °C). Despite the crude simplifications adopted in the present model, a satisfactory agreement is obtained on heat transfer rates, with some overprediction of their dependence upon the air speed.

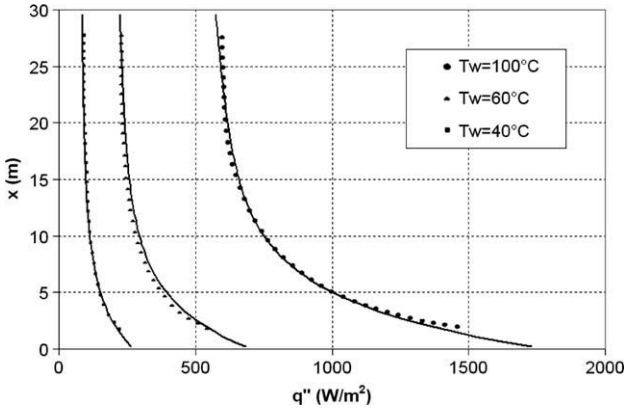

Fig. 4. Wall heat fluxes for $H = 30$ m, $s = 0.2$ m, $T_0 = 20$ °C, $x^* = H$ (dry wall) and three values of the wall temperature T_w. Solid lines: predictions by the present model using $a = 1.5$, $b = 0.18$ for the entrance effects multiplier in Eq. (19); symbols: predictions by the CFX-4 code.

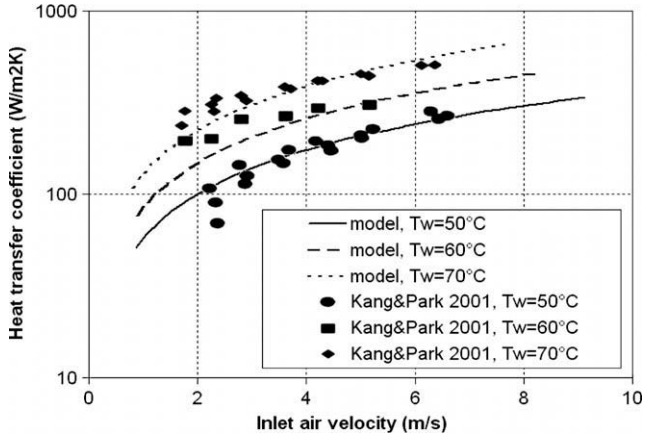

Fig. 5. Average wall heat transfer coefficient for $H = 2$ m, $s = 0.1$ m, $T_0 = 25$ °C, $x^* = 0$ (completely wet wall) and three values of the wall temperature T_w. Lines: predictions by the present model; symbols: experimental results by Kang and Park [4].

4. Results and discussion

4.1. Typical vertical profiles

As an example of the results provided by the computational model, Fig. 6 reports typical predictions obtained for a reference case characterized by $T_0 = 283.15$ K, $m_0 = 0.003$, $T_w = 373.15$ K, $H = 30$ m, $s = 0.2$ m, $K = 5$, atmospheric pressure and for two dry-out locations, $x^* = H/2$ (bottom half of the wall dry, top half wet) and $x^* = 0$ (completely wet wall). In Fig. 6(a), vertical profiles of humidity m (solid lines) and saturation humidity m_{sat} (broken lines) are shown. It can be observed that in either case the air humidity attains and exceeds saturation shortly above the dry-out location x^*, giving rise to the formation of mist in the upgoing air. In Fig. 6(b), vertical profiles of humid air temperature T_a are reported; in the case $x^* = H/2$ the existence of three different trends in the $T_a(x)$ profiles can be observed, corresponding respectively to dry wall ($x < 15$ m), wet wall cooled by undersaturated air ($x = 15$–17 m), and wet wall cooled by oversaturated air with mist ($x > 17$ m).

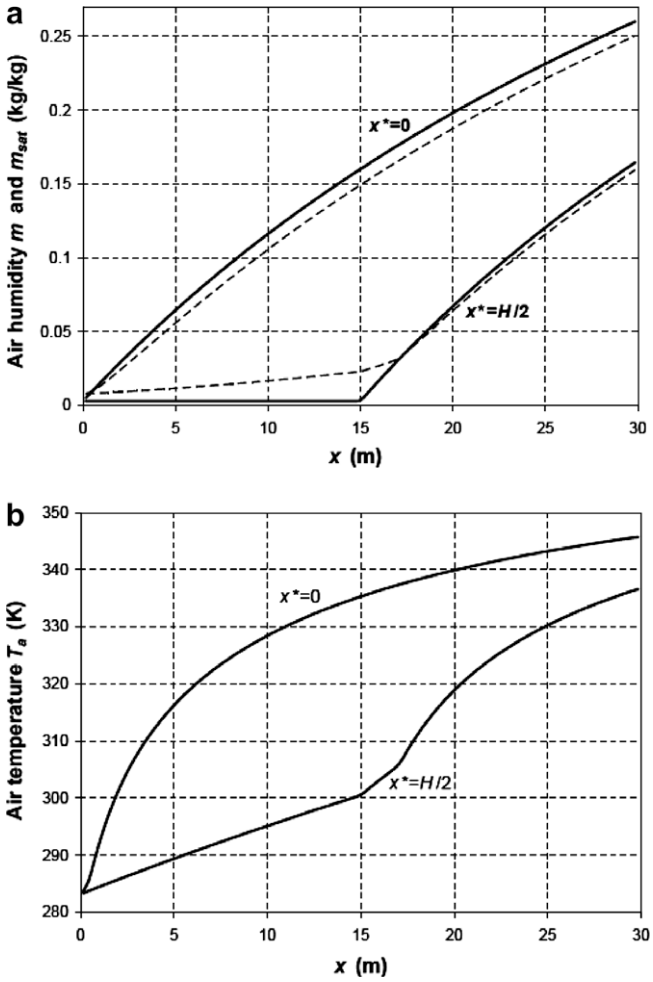

Fig. 6. Reference case ($H = 30$ m, $T_w = 373.15$ K, $T_0 = 283.15$ K, $m_0 = 0.003$, $s = 0.2$ m, $K = 5$) with dry-out locations $x^* = H/2$ or $x^* = 0$ (completely wet wall): (a) vertical profiles of air humidity m (solid lines) and saturation humidity m_{sat} (broken lines); (b) vertical profiles of humid air temperature T_a.

In the graphs that follow, the ambient conditions are the same as for the reference case but the remaining quantities T_w, H, s, K are made to vary to show their effects on global quantities such as the air flow rate and the power subtracted to the wall.

4.2. Influence of the wall temperature

Fig. 7(a) reports the inlet air flow rate $\Gamma_{a,0}$ as a function of the wall temperature T_w (assumed uniform) for $s = 0.2$ m, $K = 5$ and three values of the wall height H in the two limiting cases $x^* = H$ (dry wall) and $x^* = 0$ (wall entirely wet by a liquid film). It can be observed that the air flow rate generally increases with the wall temperature and is much higher for a wet wall than for a dry wall. Only when the wall temperature exceeds 100 °C, giving rise to nucleate boiling of the liquid film, the inlet flow rate decreases with T_w; however, the outlet flow rate (not shown here) increases monotonically with T_w in all cases since high values of T_w are associated with very high outlet humidity, well above saturation (mist).

Fig. 7(b) reports the total power W_w subtracted to the wall under the same conditions. The use of a log scale should be noticed. In the presence of a liquid film W_w is much larger than for a dry wall, and increases much more steeply with T_w (or, better, with $T_w - T_0$). Interestingly, the increase of W_w with T_w halts for $T_w = T_{sat}$, when the film surface humidity $m_\delta = m_{sat}(T_w)$ in Eq. (10) for the evaporative mass (and heat) flux attains its maximum value of 1. For further increases of T_w beyond T_{sat} the evaporative flux remains unchanged, while a boiling mass/heat flux appears which, however, remains small until $T_w - T_{sat}$ exceeds a few K.

4.3. Influence of the channel width

Fig. 6(a) reports the total power W_w subtracted to the wall as a function of the channel width s for T_w=100 °C (uniform), $H = 30$ m, three values of K and $x^* = 0$ (wet wall) or $x^* = H$ (dry wall). An optimum width, yielding maximum heat transfer, exists in all cases; it decreases with K and (for the present data range) is 0.13–0.14 m for a dry wall and 0.18–0.26 m for a completely wet wall.

The presence of a maximum in the $W_a(s)$ curve can be explained by considering the behaviour of the inlet humid air flow rate $\Gamma_{a,0}$ as a function of s, reported in Fig. 8(b) for three values of the localized resistance K (3, 5 and 10) and $x^* = 0$ (completely wet wall). Since the Dittus–Bölter correlation and the heat–mass transfer analogy were used, Eqs. (19)–(22), one has $h, h_m \sim (\Gamma_{a,0})^{0.8}/s$. Therefore, in the s ranges in which the slope of the $\Gamma_{a,0}(s)$ curve is larger or smaller than 1/0.8 = 1.25, the subtracted power W_a respectively increases or decreases with s, and is maximum when this slope is equal to 1.25.

4.4. Influence of the liquid film flow rate and cooling strategy

Fig. 9 reports the total power W_w subtracted to the wall as a function of the film inlet flow rate $\Gamma_{l,H}$ for $H = 30$ m, $s = 0.2$ m, $K = 5$ and different values of T_w. For each T_w, W_w starts from a small value $W_w(0)$ corresponding to a dry wall ($x^* = H$). As $\Gamma_{l,H}$ increases, the wet length $H - x^*$ grows and W_w increases about linearly with $\Gamma_{l,H}$ up to a value $\Gamma^*_{l,H}$, corresponding to the condition $x^* = 0$

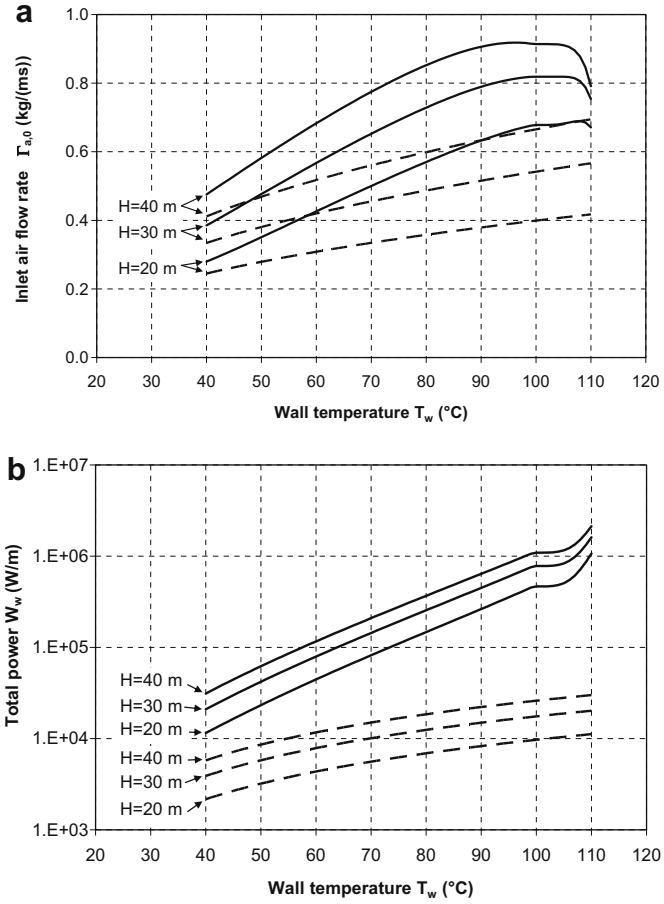

Fig. 7. Inlet air flow rate (a) and total power subtracted to the wall (b) as functions of the wall temperature T_w for $s = 0.2$ m, $K = 5$ and three values of H (20, 30, 40 m). Broken lines: dry wall ($x^* = H$); solid lines: completely wet wall ($x^* = 0$).

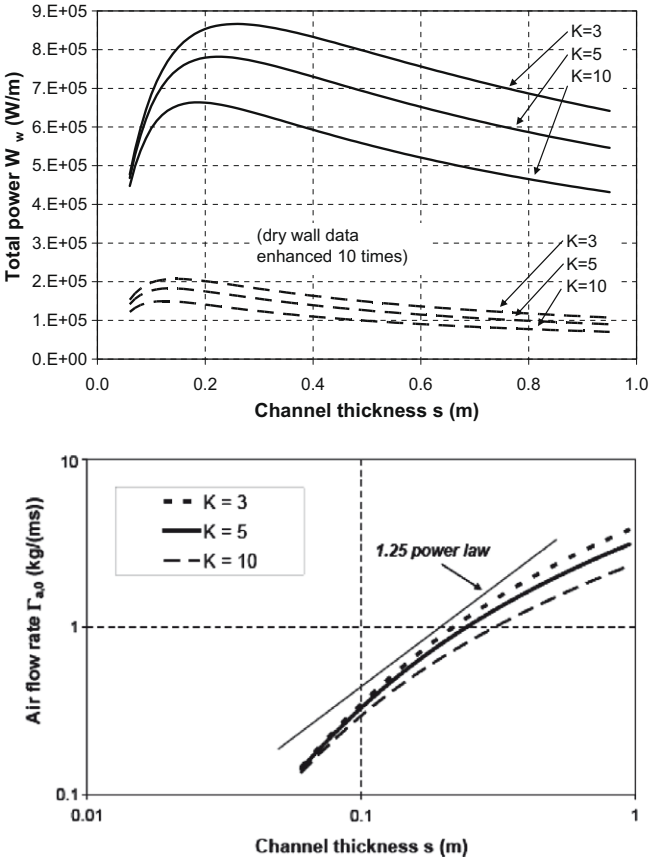

Fig. 8. (a) Total power subtracted to the wall as a function of s for $T_w = 100$ °C, $H = 30$ m and three values of K (3, 5, 10). Broken lines: $x^* = H$ (completely dry wall); solid lines: $x^* = 0$ (completely wet wall). (b) Humid air inlet flow rate as a function of the channel width for the same values of K and $x^* = 0$ (completely wet wall). The straight line corresponds to a 1.25-power law.

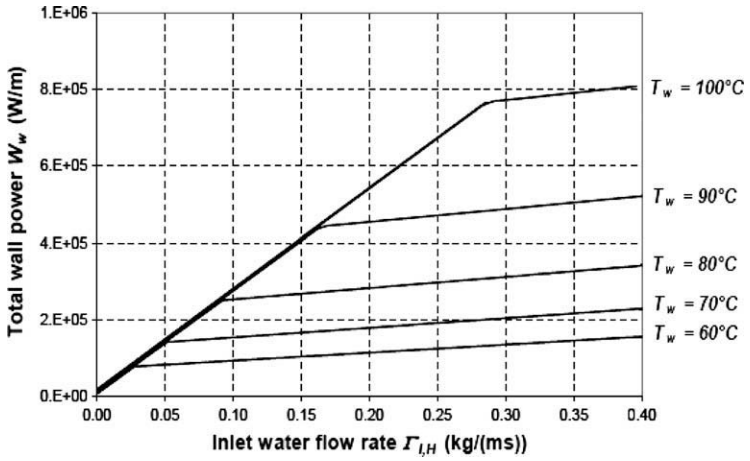

Fig. 9. Total power subtracted to the wall as a function of the film flow rate for H = 30 m, s = 0.2 m, K = 5 and different values of T_w.

(completely wet wall). For larger $\Gamma_{l,H}$, an increasing fraction of the film flow rate reaches the base of the wall in the liquid state and W_w grows more slowly, because of the sensible heat required to warm the liquid from its inlet temperature $T_{l,H}$ to the thermal equilibrium temperature T_w, whereas the power W_a transmitted to the air flow remains unchanged (Fig. 3).

Now, assume that the feed water for the liquid film is drawn from a reservoir of finite mass Q_l (per unit perimeter). Any mass flow rate $\Gamma_{l,H}$ – supposed constant – can only be provided up to a time $t_{wet} = Q_l/\Gamma_{l,H}$. The power subtracted to the wall will be $W_w(\Gamma_{l,H})$ for $0 \leqslant t < t_{wet}$ and $W_w(0)$ for $t > t_{wet}$. On the basis of results like those in Fig. 9, and assuming that T_w remains constant throughout the cooling process, the total thermal energy $E_T(t, t_{wet})$ (per unit perimeter) subtracted to the wall up to time t can be computed for different values of t_{wet}, or "cooling strategies" (Fig. 10). For each t_{wet}, the corresponding curve in Fig. 10 exhibits an abrupt change of slope at $t = t_{wet}$, associated with the transition from wet to dry cooling. The solid line is for t_{wet} equal to $t^*_{wet} = Q_l/\Gamma^*_{l,H}$, $\Gamma^*_{l,H}$ being the minimum flow rate for which the wall is completely covered by the liquid film ($x^* = 0$). For $t_{wet} > t^*_{wet}$ (i.e., $\Gamma_{l,H} < \Gamma^*_{l,H}$) the integrated thermal energy subtracted to the wall is at any time less or equal to that corresponding to $t_{wet} = t^*_{wet}$, whereas for $t_{wet} > t^*_{wet}$ (i.e., $\Gamma_{l,H} > \Gamma^*_{l,H}$) it exceeds slightly $E_T(t, t^*_{wet})$ for $t < t_{wet}$, but remains lower for any larger time. Thus, in a well defined sense, the "cooling strategy" characterized by the choice $t_{wet} = t^*_{wet}$ is *optimal*.

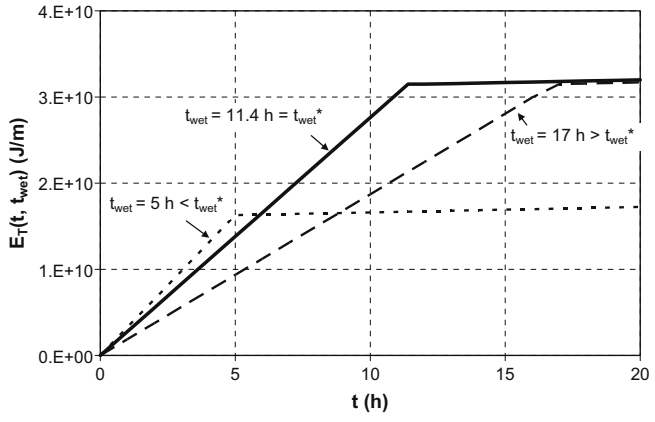

Fig. 10. Total thermal energy subtracted from the wall as a function of time for T_w = 100 °C, H = 30 m, K = 5 and different "cooling strategies".

5. Conclusions

A model was developed for the free convection cooling of a hot vertical wall, either dry or wet by a liquid water film. It was used to predict the dependence of relevant quantities, e.g., air flow rate and thermal power subtracted to the wall, on system's parameters such as wall temperature, channel height and width, localized hydraulic resistance and water supply rate.

Notably, the existence of an optimum channel width was predicted and explained. In the case of a finite water reservoir and of a constant wall temperature, the existence of an optimum "cooling strategy" was demonstrated, consisting of supplying water at the minimum flow rate which guarantees a complete coverage of the wall by the liquid film.

References

[1] R.B. Duffey, D.T.C. Porthouse, The physics of rewetting in water reactor emergency core cooling, Nucl. Eng. Des. 25 (1973) 379–394.
[2] H.J. Bruschi, The Westinghouse AP600, Atomwirtsch. Atomtech. 41 (1996) 256–259.
[3] W.T. Sha, T.H. Chien, J.G. Sun, B.T. Chao, Analysis of large-scale tests for AP-600 passive containment cooling system, Nucl. Eng. Des. 232 (2004) 197–216.
[4] Y.M. Kang, G.C. Park, An experimental study on evaporative heat transfer coefficient and applications for passive cooling of AP600 steel containment, Nucl. Eng. Des. 204 (2001) 347–359.
[5] W.-M. Yan, Evaporative cooling of liquid film in turbulent mixed convection channel flows, Int. J. Heat Mass Transfer 41 (1998) 3719–3729.
[6] I. Arshavski, Y. Nekhamkin, S. Olek, E. Elias, Conjugate heat transfer during falling film evaporation, Int. Commun. Heat Mass Transfer 22 (1995) 271–284.
[7] S.G. Bankoff, S.C. Lee, A critical review of the flooding literature, in: G.F. Hewitt, J.M. Delhaye, N. Zuber (Eds.), Multiphase Science and Technology, Hemisphere–McGraw-Hill, New York, 1986.
[8] O.L. Pushkina, Y.L. Sorokin, Breakdown of liquid film motion in vertical tubes, Heat Transfer Sov. Res. 1 (1969) 56–64.
[9] B. Ramaswamy, S. Krishnamoorty, S.W. Joo, Three-dimensional simulation of instabilities and rivulet formation in heated falling films, J. Comp. Phys 131 (1997) 70–88.
[10] M.S. El-Genk, H.H. Saber, Minimum thickness of a flowing down liquid film on a vertical surface, Int. J. Heat Mass Transfer 44 (2001) 2809–2825.
[11] V.A. Grigoriev, V.M. Zorin (Eds.), Heat and Mass Transfer. Thermal Experiment Reference Book, Energoizdat, Moscow, 1982.
[12] M. Ciofalo, Local effects of longitudinal heat conduction in plate heat exchangers, Int. J. Heat Mass Transfer 50 (2007) 3019–3025.
[13] C.H. Song, D.-Y. Lee, S.T. Ro, Cooling enhancement in an air-cooled finned heat exchanger by thin water film evaporation, Int. J. Heat Mass Transfer 46 (2003) 1241–1249.
[15] R.H. Perry, D.W. Green, Perry's Chemical Engineers' Handbook, McGraw-Hill, Singapore, 1984.
[16] U.K. Committee on the Properties of Steam, UK Steam Tables in SI Units 1970, Edward Arnold, London, 1970.
[17] Noauthor, CFX-4.2: Solver, CFX International, Harwell Laboratories, UK, 1997.